

## Tailored Fuel Injection within a Mach 12 Shape Transitioning Scramjet

W. O. Landsberg<sup>1</sup>, J. E. Barth<sup>1</sup>, A. Veeraragavan<sup>1</sup>, V. Wheatley<sup>1</sup> and M. K. Smart<sup>1</sup>

<sup>1</sup>Centre for Hypersonics  
The University of Queensland, Queensland 4072, Australia

### Abstract

Three-dimensional computational fluid dynamic simulations were performed for the Mach 12 Rectangular-to-Elliptical Shape-Transitioning scramjet. Present injector arrangements at the combustor entrance displayed low jet penetration, resulting in a oxygen-based combustion efficiency of 84.9%. It is proposed to convert three cowl-side injectors into one larger injector located further upstream. To support this, injector configurations were investigated computationally, taking injectors optimised for penetration at lower Mach numbers, and evaluating their performance at higher Mach number flight conditions. It was determined that reduced performance of these optimised injectors was encountered at scramjet flight conditions above their design point, with circular injectors at equal or greater injection angles displaying greater penetration and mixing capabilities.

### Introduction

Airbreathing scramjets offer significant efficiency and operability benefits for hybrid satellite launch vehicles, compared to current rocket-based systems. Smart and Tetlow [1] showed that for small satellite launches, payload mass fractions of 1.47% were achievable for hybrid rocket-scramjet configurations, with a hydrogen fuelled scramjet engine accelerating through Mach 6-12. This compares favourably to the 0.9% offered by conventional rocket-based systems as oxidisers need not be carried on-board. Scramjets offer reusability benefits, translating to the potential for “aircraft-like operation” with the desired higher reliability and more economical delivery of payloads to orbit [2].

These studies, however, demanded scramjet engines capable of accelerating through a Mach number range, with an engine capable of Mach 12 flight required. However, few studies have characterised such engines sufficiently. Preliminary investigations indicated airframe integrated, modular systems are required, whereby the vehicle forebody performs initial shock compression [3]. The Mach 12 Rectangular-to-Elliptical Shape-Transitioning (M12REST) inlet was designed by Smart [3] to meet this need: it combines a rectangular capture area for side-by-side mounting, and an elliptical combustor for structural efficiency (figure 1). The highly swept leading edges and notched cowl allow for engine operation over a Mach number range, with simple fixed geometry [4].



Figure 1: Mach 12 REST scramjet test article

At Mach 12 speeds, however, airflow residence time within the combustor approaches air-fuel mixing and reaction time-

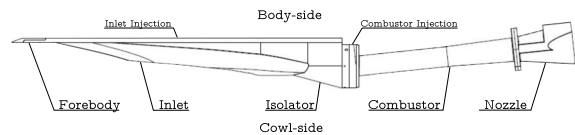


Figure 2: Mach 12 REST scramjet schematic adapted from [5]

scales [6]. Hence, fuel injection schemes, tailored to interact favourably with the non-uniform flow structures within the M12REST flow-path are required to achieve a suitably high combustion efficiency.

### Current Full Flow-path

Computational fluid dynamics (CFD) was utilised to analyse the M12REST flow-path with current injector arrangements. Three porthole injectors are located in the inlet, downstream of the first compression surface, with five porthole injectors located immediately upstream of the combustor. Half of the full M12REST flow-path was meshed, taking advantage of the body-cowl symmetry plane. The final combustor mesh contained 44.15 Million cells. Figure 3 shows the grid around the combustor step, kept fine in order to resolve the evolution of the injected fuel plumes.

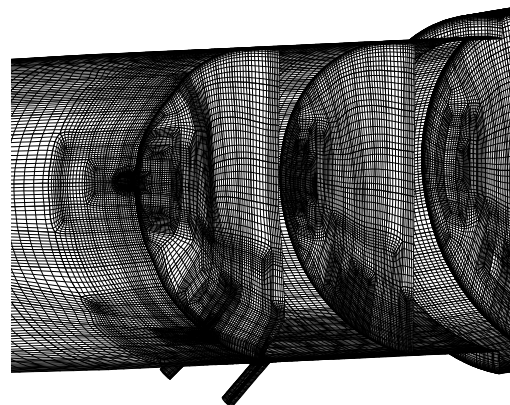


Figure 3: Grid surrounding combustor fuel injectors

### Solver & Mesh

Solutions to the Reynolds-averaged Navier-Stokes (RANS) equations were computed utilising the state-of-the-art compressible flow solver, US3D, developed by Candler's group [7]. US3D is capable of accurate simulations of high Mach number scramjet flows, handling complex geometries, strong shocks, turbulence and non-equilibrium thermochemistry [8, 9]. The Spalart-Allmaras [10] turbulence model is utilised, with boundary layers assumed to be fully turbulent throughout the domain. While a grid convergence study was completed for the inlet mesh alone [8], the combustor mesh was constructed in the same manner, and will be compared with experimental results at a later date. The flow through the engine was solved assuming a fuel equivalence ratio of 1.24, and converged by 6 orders of magnitude.

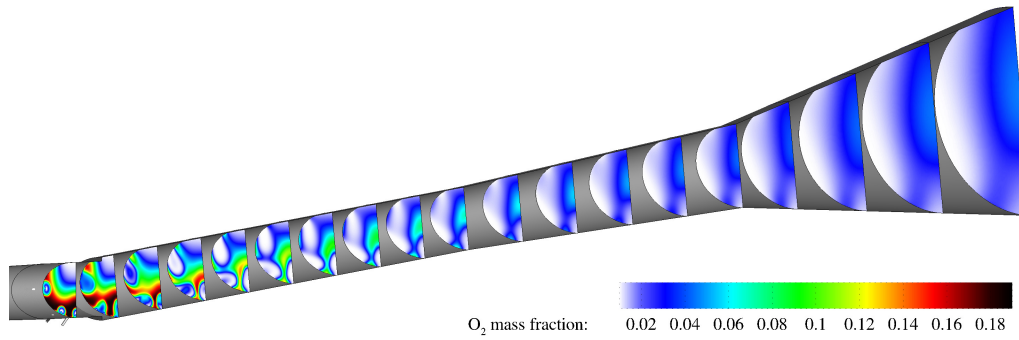


Figure 5: Centre-plane and cross-planes showing  $O_2$  mass fraction (white=0) from M12REST RANS simulation

## Results

To increase air-fuel mixing, we inject 30% of the hydrogen fuel in the inlet; the remainder at the combustor entrance. A combination of greater mixing length, interaction with the turbulent boundary layer [8] and shock-fuel plume interactions at the combustor entrance [9] result in this fuel being well mixed as it enters the combustor. This inlet injected fuel ignites locally and the flame subsequently propagates across the entire fuel plume, resulting in a stream of hot, radical laden flow to pilot ignition of the combustor injected fuel. The benefits of this inlet fuelling outweigh the increased inlet drag of less than 5%.

However, the amount of fuel injected at the inlet is limited, as fuel is only able to mix with air on the body-side of the engine [8], as shown in figure 4, and too much injection leads to engine unstart. Hence, injection is required at the combustor entrance; however, current injector arrangements visible in figure 4, fail to optimally mix with the available oxygen. Jet penetration of the three cowl-side injectors was found to be lower than required, leaving unreacted air flowing through the core of the engine cross-section. This is shown in figure 5 with a high  $O_2$  mass fraction core flow present through the engine. Despite this behaviour, the global oxygen-based combustion efficiency of the engine was found to be 84.9%.

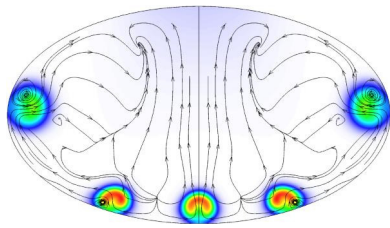


Figure 4: In-plane streamlines and  $H_2$  mass fraction at combustion chamber entrance

To make full use of this captured oxygen, it is proposed to tailor the three cowl-side injectors to penetrate further into this oxygen rich flow. As intrusive devices such as struts are unsuitable at high speeds due to heating loads and losses [11], injectors optimised for fuel penetration are to be analysed with the aim of converting the cowl-side injectors into one larger injector, located further upstream. However, while the literature includes a broad range of fuel injection studies, few have been performed at the high enthalpy flows encountered within the M12REST isolator. Ogawa and Boyce have performed extensive optimisation studies [12], however these were targeted at Mach 8 scramjet conditions. To make use of these studies, we will numerically evaluate the performance, at the conditions present in the M12REST isolator, of injectors optimised for maximum penetration in a Mach 8 scramjet. The resulting fuel jet penetration height, mixing efficiency and total pressure losses are key performance parameters that will be used to compare the new injector performance to that of standard circular portholes.

## Injector Simulation Methodology

Sonic, chemically frozen fuel injection into an incoming cross flow is modelled. Flow conditions taken from Ogawa and Boyce [12], together with those extracted from the M12REST isolator, are listed in table 1. Hydrogen fuel is injected, with both air and hydrogen assumed to be calorically perfect with a ratio of specific heats of 1.4.

		Mach number	P (kPa)	T (K)
Mach 8	At inlet	7.63	1.70	254
	At injection (M8)	5.63	7.69	433
Mach 12	Freestream	9.28	0.886	359
	At inlet (M12)	5.31	32.6	1060
Hydrogen	Injection	1	1611	250

Table 1: Cross flow conditions at injection

A simple flow channel of length (L) 100mm, width (W) 14.2mm and height (H) of 32mm is modelled, as shown in figure 6. A symmetric boundary condition is utilised at the jet centreline, as well as at  $y=14.2\text{mm}$  to model injector spacing of 28.4mm. Symmetry is imposed at the upper edge ( $z=32\text{mm}$ ) to ensure mass flow is conserved. An isothermal 300K wall is imposed, characteristic of shock tunnel test times. A fuel injector is modelled 10mm downstream from the air inflow boundary ( $L_0$ ), with sonic choked flow at the exit plane. A separate CFD computation was performed at each condition to develop a turbulent boundary layer air inflow profile. Boundary layer thicknesses of 2.77mm and 1.5mm (based on  $0.99U_\infty$ ) were obtained for the M8 and M12 conditions respectively, to match Ogawa's simulations, and the M12REST cowl-side flow.

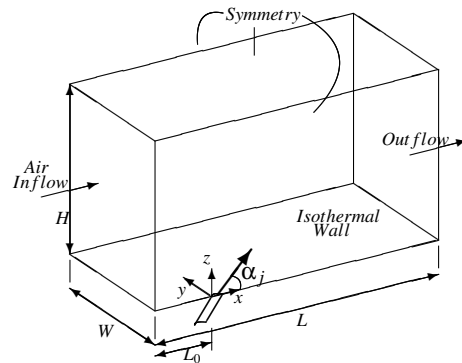


Figure 6: Injector Configuration

The aim of this study is to replace the three cowl-side injectors with a single injector, located further upstream. Thus, the combined mass flow from these injectors of 1.5g/s (0.75g/s within the half domain modelled) was implemented for this simulation. With the intent to increase fuel penetration, the injector most optimised for penetration was taken from [12] (labelled

'30-Ellip'). Circular baseline injectors were also modelled. As the mass flow in this study differs from [12], the effective injector radius, defined as  $r_j = \sqrt{A_{nj}/\pi}$  where  $A_{nj}$  is the cross-sectional area normal to the jet, was altered, while maintaining the hydrogen fluid properties. The injector geometry utilised in this investigation is described in table 2, with elliptical aspect ratio (AR) relative to the jet normal.

Injector	$\alpha_j$	AR	$r_j$	$p_j$	$T_j$
45-Circ	45.0°	1	0.504mm	1611kPa	250K
30-Circ	30.2°	1	0.504mm	1611kPa	250K
30-Ellip	30.2°	3.32	0.504mm	1611kPa	250K

Table 2: Injector geometry

### Computational Fluid Dynamics

US3D is utilised in this study for consistency. High fidelity, structured grids were generated using GridPro v5.6. Wall adjacent cells were set to  $1\mu\text{m}$ , giving a wall normal non-dimensionalised distance of less than 0.8 for  $z^+$ . Mesh convergence was determined using the method of Stern *et al.* [13]. Based on this model, a 1.7 million cell mesh for the 45° circular injector should match an infinitely fine grid to within 3.1% for fuel plume centroid penetration distance, and 6.5% for pressure losses. Hence, it is assumed that for a relative comparison between injectors, meshes of this order of accuracy are suitable.

### Injector Results

Results are presented for the key metrics of fuel penetration, spanwise fuel spread, mixing efficiency and stagnation pressure losses for each injector. Here, fuel penetration is defined as

$$h_p = \max(z|_{Y_{H_2} > 0.1Y_{H_2}^s}), \quad (1)$$

where  $Y_{H_2}^s$  is the stoichiometric mass fraction of hydrogen for air combustion ( $0.1Y_{H_2}^s = 0.0029$ ). Results are presented in figure 7, with distances normalised to the jet diameter ( $D_j = 1.01\text{mm}$ ).

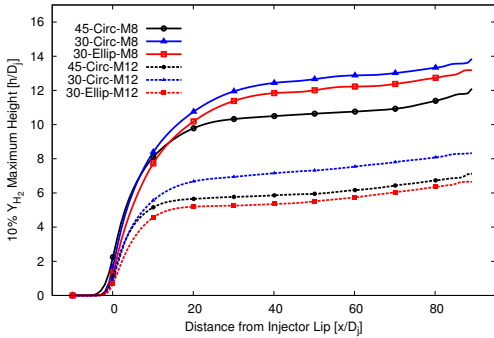


Figure 7: Penetration of 10%  $Y_{H_2}^s$  vs streamwise location

As expected from [12], the elliptical injector outperformed the baseline circular injector for the M8 condition; however the opposite was true for the M12 condition. Further, the 30° circular injector had the best performance for each condition. The magnitude of the difference in penetration, for each injector, between each flow condition may be due to the effect of the jet-to-freestream momentum flux ratio, given as

$$J = \frac{(\rho U^2)_{jet}}{(\rho U^2)_{air}} = \frac{(\gamma p M^2)_{jet}}{(\gamma p M^2)_{air}}, \quad (2)$$

yielding values of 6.52 and 1.76 for injection pressures of 1611kPa into the M8 and M12 conditions, respectively. Previous studies have indicated that penetration increases as a function of  $J$  [14]. To determine why the elliptical injector did not

display improved performance in the M12 condition, the mass-flow weighted average plume height was evaluated along the streamwise direction, as per equation (3)

$$h_{\oplus} = \frac{\int (\rho_{H_2} u z) dA}{\int (\rho_{H_2} u) dA}, \quad (3)$$

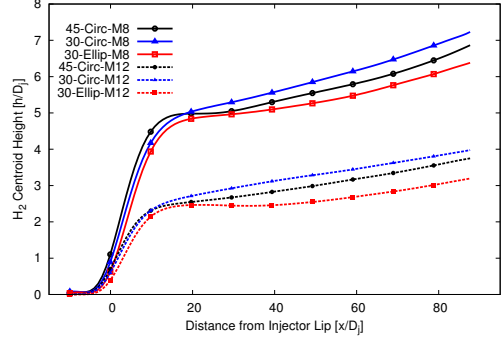


Figure 8: Fuel centroid height vs streamwise location

Again, the 30° circular injector achieved the greatest performance universally. In contrast to the 10%  $Y_{H_2}^s$  penetration height, the centroid height of the fuel plume was higher for the 45° circular injector than the 30° elliptical injector for each condition. The slope for the M8 condition indicated that the 45° circular injector would depart further from the elliptical injector further downstream. The slopes were approximately equal for the M12 condition. Spanwise fuel spread at the exit plane ( $L=90\text{mm}$ ), defined as equation (4), is shown in figure 9.

$$w_p = \frac{\int (\rho_{H_2} u y) dA}{\int (\rho_{H_2} u) dA}, \quad (4)$$

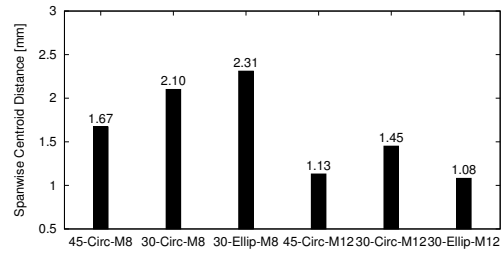


Figure 9: Spanwise fuel spread at  $x=L$

Comparing figures 7, 8 and 9, it appears the 30° elliptical injector produced a highly diffuse fuel plume for the Mach 8 condition. The 30° circular injector appeared to perform similarly for the M12 condition. Thus, the air-fuel mixing efficiency at the exit plane is determined as per equation (5)

$$\eta_m = \frac{1}{\dot{m}_{H_2}} \int \min\left(Y_{H_2}, \frac{Y_{H_2}^s}{Y_{O_2}^s} Y_{O_2}\right) d\dot{m}, \quad (5)$$

where  $Y_{H_2}^s = 0.029$  and  $Y_{O_2}^s = 0.228$

The improved mixing for the 30° elliptical injector and 30° circular injector at the M8 and M12 conditions respectively is evident. It is likely that turbulent interactions between the freestream and fuel plume shear layer improved vertical penetration of trace amounts of hydrogen, due to the shape and angle of the elliptical injector, compared to the 45° circular injector. This same injector clearly does not have the same effect within a higher dynamic pressure flow, with each circular injector displaying improved performance across both penetration metrics.

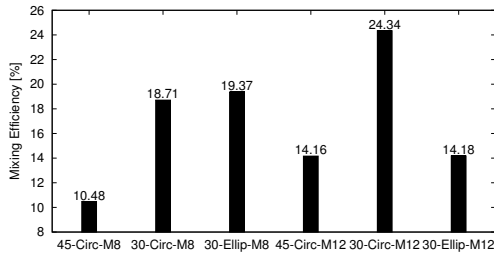


Figure 10: Mixing efficiency at exit plane ( $x = 90\text{mm}$ )

The  $30^\circ$  circular injector displayed vastly improved mixing performance. Hence, a more robust injector design is required for any accelerating scramjet, flying across a broad range of Mach numbers. Interestingly, the mixing efficiency of each injector at the M12 condition outperformed the  $45^\circ$  circular injector at the M8 condition. This may be due to the higher Reynolds number for the M12 condition of  $8.61 \times 10^6/m$  vs  $6.05 \times 10^6/m$ , which would increase the level of turbulence along the shear layer between the fuel plume and freestream. Aside from penetration, injectors are required to minimise pressure losses. Stagnation pressure was determined by integrating slices along the streamwise direction, and normalised to the inflow as per equation (6)

$$p_{t_{\text{recovery}}} = \frac{\int_x p_t d\dot{m}}{\int_{x=-L_0} p_t d\dot{m}}, \quad (6)$$

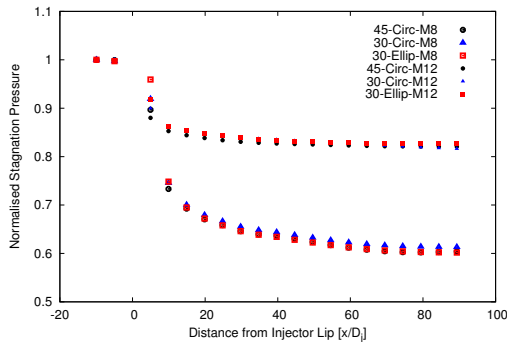


Figure 11: Stagnation pressure vs streamwise location

Due to the reduced penetration distance for the M12 scramjet condition, total pressure losses (relative to the inflow) were less than those for the M8 condition. Negligible differences were encountered between each injector type, at the same condition.

## Conclusion

Numerical analysis of the M12REST half-scale flow-path, with current injector arrangements was performed. It was found that the oxygen based combustion efficiency was lower than optimal. Cowl-side injectors displayed reduced penetration, contributing to this reduced combustion efficiency. Recommendations have been made convert these three cowl-side injectors into one, located further upstream.

Preliminary fundamental studies have been performed on injector types optimised for penetration at Mach 8 scramjet conditions, together with baseline circular injectors. Sonic hydrogen was injected into a cross flow characteristic of Mach 8 and 12 scramjet flight conditions. The same improvement in penetration displayed at the M8 condition was not encountered at the higher enthalpy condition, with reduced performance compared to circular injectors, at equal and greater pitch angles. Performance metrics indicated that the circular injector, inclined at  $30^\circ$  displays significantly improved performance at the M12 condition, relative to the baseline injectors.

## Acknowledgements

This research was undertaken with the assistance of resources provided at the NCI National Facility through the National Computational Merit Allocation Scheme (project dc7) supported by the Australian Government and was supported under Australian Research Council's LIEF funding scheme (project number LE120100181). AV also acknowledges support from the ARC under project DP130102617.

## References

- [1] Smart, M.K and Tetlow, M.R., Orbital delivery of small payloads using hypersonic airbreathing propulsion *Journal of Spacecraft and Rockets*, **46**, 2009, 117–125
- [2] Flaherty, K.W., Andrews, K.M. and Liston, G.W., Operability benefits of airbreathing hypersonic propulsion for flexible access to space *Journal of Spacecraft and Rockets*, **47**, 2010, 280–287
- [3] Smart, M.K., Design of three-dimensional hypersonic inlets with rectangular-to-elliptical shape transition *Journal of Propulsion and Power*, **15**, 1999, 408–416
- [4] Moule, Y. and Smart, M.K., Performance Analysis of a Mach 12 Scramjet at Off-Design Conditions *Journal of Propulsion and Power*, **29**, 2012, 282–285
- [5] Smart, M., Scramjets, *The Aeronautical Journal of the Royal Aeronautical Society*, **111**, 2007, 605–619
- [6] Petty, D.J., Wheatley, V., Smart, M.K. and Razzaqi, S.A., Effects of Oxygen Enrichment on Scramjet Performance *AIAA journal*, **51**, 2012, 226–235
- [7] Nompelis, I., Drayna, T.W. and Candler, G.V., Development of a hybrid unstructured implicit solver for the simulation of reacting flows over complex geometries *AIAA Paper*, **2227**, 2004
- [8] Barth, J.E., Wheatley, V. and Smart, M.K., Inlet Fuel Injection in a Mach 12 Shape-Transitioning Scramjet, *AIAA SciTech, National Harbor, Md, USA*, 2014, 13-17
- [9] Gehre, R., Peterson, D., Wheatley, V. and Boyce, R., Numerical investigation of the mixing process in inlet-fuelled scramjets *ISSW29: 29th International Symposium on Shock Waves*, 2013, 1–6
- [10] Spalart, P. and Allmaras, S., A one-equation turbulence model for aerodynamic flows, *30th Aerospace Sciences Meeting & Exhibit AIAA-92-0439*, 1992, 1-22
- [11] Billig, F.S., Research on supersonic combustion *Journal of Propulsion and Power*, **9**, 1993, 499–514
- [12] Ogawa, H. and Boyce, R.R., Multi-objective design optimization of fuel injection for mixing enhancement in scramjets by using surrogate-assisted evolutionary algorithms *18th AIAA/3AF International Space Planes and Hypersonic Systems and Technologies Conference*, 2012, 1–18
- [13] Stern, F., Coleman, H.W., Paterson, E.G. and Wilson, R.V., Comprehensive approach to verification and validation of CFD simulations part 1: methodology and procedures *Journal of fluids engineering*, **123**, 2001, 793–802
- [14] Tomioka, S., Jacobsen, L.S. and Schetz, J.A., Sonic injection from diamond-shaped orifices into a supersonic cross-flow *Journal of Propulsion and Power*, **19.1**, 2003, 104–114